Li *et al. Chem Synth* 2024;4:48
DOI: 10.20517/cs.2023.79

Chemical Synthesis

Research Article

Open Access

Check for updates

Fluorinated porous organic frameworks for C_2F_6/CF_4 gases separation

Yinhui Li, Yue Wu, Shanshan Wang, Yu Fu, Xiaoyu Li, Jiahui Zeng, Wenxiang Zhang*, Heping Ma*

School of Chemical Engineering and Technology, Xi'an Jiaotong University, Xi'an 710049, Shaanxi, China.

***Correspondence to:** Dr. Wenxiang Zhang, Dr. Heping Ma, School of Chemical Engineering and Technology, Xi'an Jiaotong University, No. 28 Xianning West Road, Beilin District, Xi'an 710049, Shaanxi, China. E-mail: zhangwenxiang@xjtu.edu.cn; maheping@mail.xjtu.edu.cn

How to cite this article: Li Y, Wu Y, Wang S, Fu Y, Li X, Zeng J, Zhang W, Ma H. Fluorinated porous organic frameworks for C_2F_6/CF_4 gases separation. *Chem Synth* 2024;4:48. https://dx.doi.org/10.20517/cs.2023.79

Received: 31 Dec 2023 **First Decision:** 7 May 2024 **Revised:** 4 Jul 2024 **Accepted:** 22 Jul 2024 **Published:** 9 Aug 2024

Academic Editors: Wei Li, Guangshan Zhu **Copy Editor:** Dong-Li Li **Production Editor:** Dong-Li Li

Abstract

As an indispensable raw material for silicon-based semiconductor industry, carbon tetrafluoride (CF_4) is widely used as plasma etching and cleaning gas in the manufacture of semiconductors. How to efficiently remove the C_2F_6 impurity during the CF_4 production process is a challenging task as semiconductor industry requires high-purity CF_4 gas. Herein, two fluorine-functionalized porous organic frameworks (F-POFs) named SPPOF-4F and SPPOF-8F were synthesized and used for separation of C_2F_6/CF_4 gases. Single-component gas adsorption experiments and ideal adsorbed solution theory (IAST) calculations indicate that two porous organic frameworks can selectively adsorb C_2F_6 from C_2F_6/CF_4 mixture. Molecular simulations have further complemented these experimental findings by revealing F-induced host-guest interactions between F-POFs and C_2F_6 at a molecular level. Additionally, dynamic breakthrough experiments verified that the F-POFs can capture C_2F_6 in C_2F_6/CF_4 mixture at practical conditions. These results indicate that F-POFs have great potential for application in the separation and purification of CF_4 electronic special gases.

Keywords: Porous organic framework, fluorine-functionalization, gases adsorption, adsorption separation, C_2F_6/CF_4

INTRODUCTION

Carbon tetrafluoride (CF_4) is a perfluoro-electronic specialty gas that plays an indispensable role in the production of semiconductor electronics[1-5]. The direct fluorination of carbon using F_2 gas is the most

dominant method to produce CF_4 due to the advantages of easily obtainable raw materials, a controllable process, and high yield[6-8]. In the direct fluorination of carbon, other fluorinated hydrocarbon impurities including C_2F_6 are also obtained[9]. Removing C_2F_6 impurities is a key issue to obtaining high-purity CF_4.

Facing this challenge, various methods have been employed for CF_4 purification including distillation, adsorption and membrane separation[10-12]. Cryogenic distillation is presently the predominant method for gas separation; however, its substantial investment and energy costs may not be sustainable for the removal of trace C_2F_6 impurities from CF_4[13,14]. Adsorption separation is regarded as a sustainable and eco-friendly option for the purification of gases, offering potential energy savings[15-25]. A variety of porous adsorbents, including activated carbon (AC), zeolites, porous alumina, metal-organic frameworks (MOFs), and some porous organic frameworks (POFs)[26-30], have been documented for the adsorption and separation of perfluorinated gases[30-39]. Compared to traditional porous adsorbents such as zeolite and MOFs[40-43], POFs with strong covalent bonds show excellent acid resistance[44-47], which are more suitable used in CF_4 purification as fluorination of carbon using F_2 usually accompanied by HF gas impurities[9].

Herein, we designed and synthesized two fluorine-functionalized POFs (F-POFs), namely SPPOF-4F and SPPOF-8F, to selectively remove C_2F_6 impurities from CF_4. Single-component adsorption experiments and dynamic breakthrough experiments demonstrated that SPPOF-4F and SPPOF-8F were able to capture C_2F_6 from C_2F_6/CF_4 gas mixtures, and in particular, SPPOF-8F showed an ideal adsorbed solution theory (IAST) selectivity of 8.26 when C_2F_6 : CF_4 is 1:99. In addition, density-functional theory (DFT)-based theoretical calculations provide insights into the internal mechanism of selective adsorption of C_2F_6 in F-POFs at the molecular level.

EXPERIMENTAL

Chemicals

Chemicals 2,2',7,7'-Tetrabromo-9,9'-spirobifluorene (referred to as SP-4Br), 1,2,4,5-tetrafluorobenzene (referred to as Benz-4F), 4h,4'h-octafluorobiphenyl (referred to as Biph-8F) and $Pd(OAc)_2$ were procured from Aladdin. The compound Di-tert-butyl(methyl)phosphonium tetrafluoroborate was obtained from Bidepharm. Anhydrous K_2CO_3 was acquired from Macklin. High-purity (99.99%) C_2F_6 and CF_4 were sourced from Wuhan Newradar Special Gas Co. Ltd. Unless specifically specified, all chemicals involved in this study are readily available for commercial purchase and utilized without additional purification.

Synthesis

SPPOF-4F was synthesized following previously reported literature methods with minor modifications[48]. In a typical synthesis route, SP-4Br (316.0 mg,0.5 mmol), Benz-4F (111.6 μL, 1.0 mmol), anhydrous K_2CO_3 (276.4 mg, 2.0 mmol) and $P(t\text{-}Bu)_2Me\text{-}HBF_4$ (24.7 mg, 0.1 mmol) were dissolved in anhydrous dimethylacetamide (DMAc, 15 mL). $Pd(OAc)_2$ (11.2 mg, 0.05 mmol) was introduced into the mixture in a nitrogen-filled environment following degassing through freeze-pump-thaw cycles three times. The reaction mixture was agitated for 48 hours in a nitrogen environment at 120 °C. After the reaction had been cooled to room temperature, the resultant mixture was subsequently transferred into 150 mL of deionized water. The resulting precipitates were filtered and subsequently washed with deionized water, methanol and tetrahydrofuran (THF). The dark green solid was obtained after being Soxhlet-extracted with methanol for 24 h followed by THF for another 24 h and then dried overnight in a vacuum oven at 100 °C. In the end, the dark gray solid SPPOF-4F was acquired. A final solid of 266 mg was obtained with a yield of 90%.

The synthesis of SPPOF-8F was carried out following the identical procedure used for SPPOF-4F. Initially, SP-4Br (316.0 mg, 0.5 mmol), Biph-8F (298.2 mg, 1.0 mmol), $P(t\text{-}Bu)_2Me\text{-}HBF_4$ (24.7 mg, 0.1 mmol), and

K_2CO_3 (276.4 mg, 2.0 mmol) were dissolved in 15 mL of anhydrous DMAc. After degassing by freeze-pump-thaw cycles under a nitrogen atmosphere, $Pd(OAc)_2$ (5.61 mg, 0.025 mmol) was subsequently added to the mixture. Then, the reaction mixture was agitated for 48 h in a nitrogen environment at 120 °C. After the reaction had been cooled to room temperature, the resultant mixture was subsequently transferred into 150 mL of deionized water. The solid particles were subsequently filtered and sequentially washed with deionized water, methanol and THF. The dark green solid was obtained after being Soxhlet-extracted with methanol for 24 h followed by THF for another 24 h and then dried overnight in a vacuum oven at 100 °C. In the end, the dark gray solid SPPOF-8F was acquired.

Analytical characterization

The Fourier transform infrared (FT-IR) spectra were acquired using a Nicolet iS50 attenuated total reflectance IR spectrometer. The powder X-ray diffraction (PXRD) patterns of the samples were obtained with a Bruker D8 Advance instrument. Scanning electron microscopy (SEM) images were captured using an MAIA3LMH microscope. Elemental analysis was conducted via Aztec X-maxN 50mm^2 energy dispersive spectroscopy (EDS) analyzer. The ^{13}C solid-state cross polarization/magic angle spinning nuclear magnetic resonance (CP/MAS NMR) spectra are collected by Bruker 400M. The X-ray photoelectron spectroscopy (XPS) tests were conducted by Thermo Scientific K-Alpha+. The thermogravimetric analysis (TGA) of two F-POFs was carried out using a TGA instrument (type: NETZSCH TG 209F3) under an air atmosphere and a temperature range from 35 to 800 °C at a heating rate of 10 °C/min. All samples were weighed within the range (5~6 mg). Nitrogen adsorption/desorption isotherms at 77 K were obtained using a Micromeritics ASAP 2460 analyzer. C_2F_6 and CF_4 isotherms at various temperatures were recorded with a BSD-PM2 gas adsorption Analyzer from Beishide Instrument Technology (Beijing) Co., LTD. Before each measurement, the samples (approximately 150 mg) were subjected to heating at 393.15 K under dynamic vacuum conditions for a duration of 12 h. High-purity (≥ 99.99%) gases (C_2F_6 and CF_4) were utilized for the isotherm measurements.

Computational details

Isotherms fitting

Single-component isotherms of C_2F_6 and CF_4 were modeled using a dual-site Langmuir-Freundlich model across the entire pressure range (0~1 bar).

$$N = A_{11}\frac{B_{11}\times P^{C_{11}}}{1+B_{11}\times P^{C_{11}}} + A_{21}\frac{B_{21}\times p^{C_{21}}}{1+B_{21}\times p^{C_{21}}} \quad (1)$$

Here, N is molar loading of gas (mmol·g^{-1}), A is saturation capacity (mmol·g^{-1}), B is Langmuir constant (kPa^{-1} or kPa^{-C}), C is Freundlich constant, and P represents the equilibrium pressure of the bulk gas in contact with the adsorbed phase (bar).

Isosteric heat of adsorption

The adsorption data for C_2F_6 and CF_4 were modeled using a virial-type expression consisting of temperature-independent parameters a_i and b_i:

$$\ln(P) = \ln(N) + \frac{1}{T_i}\sum_{i=0}^{m} a_i N^i + \sum_{i=0}^{n} b_i N^i \quad (2)$$

where P represents pressure in millimeters of mercury (mmHg), N denotes the amount adsorbed in milligrams per gram (mg/g), T_i stands for temperature in Kelvin (K), and m and n are the respective parameters a_i and b_i.

The isosteric heat of adsorption, Q_{st}, is formally defined as:

$$Q_{st} = -R\sum_{i=0}^{m} a_i N^i \quad (3)$$

where R is the gas constant, 8.314 J·mol^{-1}·K^{-1}.

IAST calculations

The selectivity of C_2F_6/CF_4 in a mixture gas can be defined as:

$$S = (x_1/y_1)/(x_2/y_2) \quad (4)$$

where x_1 and y_1 (x_2 and y_2) represent the molar fractions of C_2F_6 and CF_4 in the adsorbed and bulk phases, respectively. The values of x_1 and x_2 were determined using the IAST developed by Myers and Prausnitz.

Theoretical simulation calculation

Simulation calculations were conducted to investigate the adsorption and separation mechanism of C_2F_6 and CF_4 in the POFs. The interaction energy (E_{Int}) distribution and the energetic minimal configuration are simulated using the Sorption module of Materials Studio. The Mulliken atomic charge and the electrostatic potential distribution of gases, POFs and POFs@gas were calculated by the DMol^3 module in Materials Studio.

RESULTS AND DISCUSSION

Structure and characterization

In a typical synthesis process, SPPOF-4F and SPPOF-8F were synthesized through the polycondensation of aryl fluorides with aryl bromide as per previously reported methods with minor adjustments[48] [Scheme 1]. In order to confirm the functional group composition of SPPOF-4F and SPPOF-8F, Fourier infrared transform (FT-IR) analysis was performed and the results were shown in Figure 1. In the FT-IR spectra, distinct C–F characteristic absorption peaks were observed for the aryl fluoride monomer, with a stretching vibration peak near 1,200 cm^{-1} corresponding to C–F. Furthermore, SP-4Br displayed a prominent peak at approximately 520 cm^{-1} associated with the stretching vibration of C–Br bonds. A comparison of the monomer spectra reveals the absence of characteristic absorption peaks attributed to C–Br bonds in the spectra of SPPOF-4F and SPPOF-8F, indicating successful condensation of aryl fluoride and aryl bromide. Additionally, the stretching vibration peaks related to C–F bonds are evident in the spectra of both products, suggesting successful preservation of C–F bonds during the polycondensation reaction[49]. The crystallinity of the POFs was assessed using PXRD, revealing amorphous patterns for both SPPOF-4F and SPPOF-8F polymers [Supplementary Figure 1].

The chemical bonds and elemental compositions of the two F-POFs were examined using XPS for analysis. As shown in Supplementary Figure 2, the XPS spectra of SPPOF-4F and SPPOF-8F revealed the existence of carbon and fluorine in their compositions, featuring binding energies of 285.1 and 687.1 eV for carbon and fluorine, respectively. The enlarged portions of the XPS spectra in the C1s segment are shown in Figure 1C and D.The findings suggest that the C–F bonding signals in SPPOF-8F are notably more pronounced than those in SPPOF-4F, likely due to the higher concentration of F atoms present in SPPOF-8F. To further validate the molecular structures of the two polymers, ^{13}C solid-state CP/MAS NMR characterization was

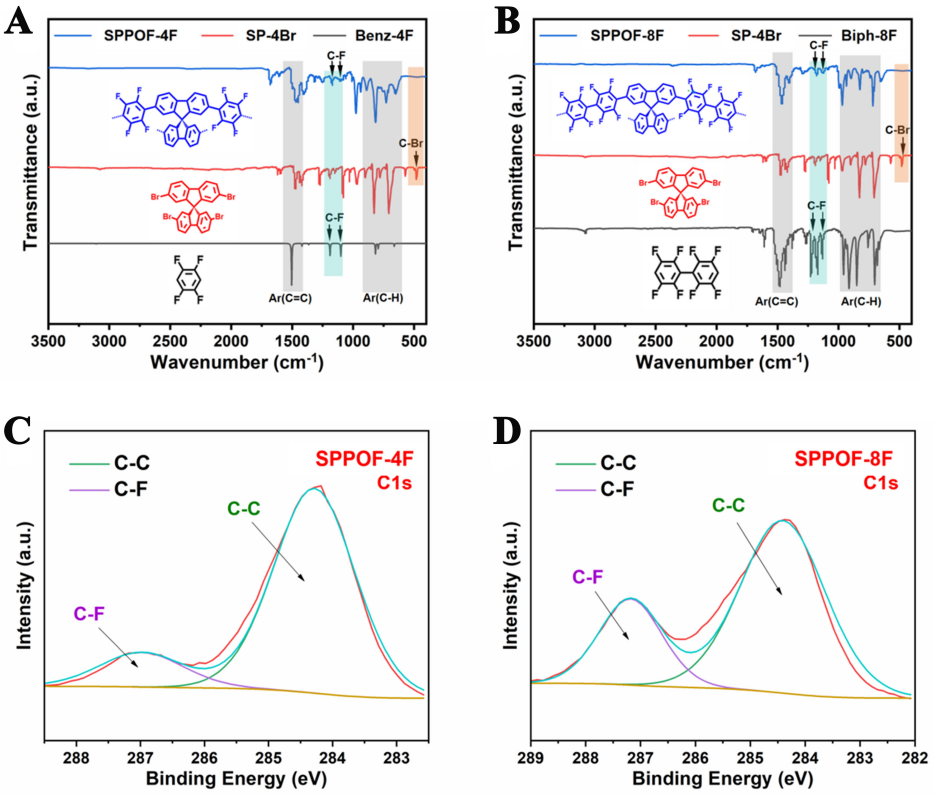

Figure 1. FT-IR spectra of monomers and POFs: (A) SPPOF-4F; (B) SPPOF-8F; and XPS spectra enlarged views of C1s in (C) SPPOF-4F and (D) SPPOF-8F. FT-IR: Fourier transform infrared; POFs: porous organic frameworks; XPS: X-ray photoelectron spectroscopy.

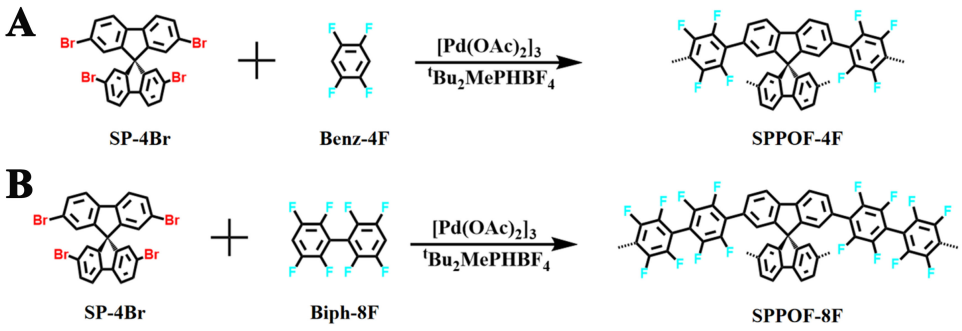

Scheme 1. Synthetic route of (A) SPPOF-4F and (B) SPPOF-8F.

conducted. The ^{13}C NMR spectra and corresponding C-resonance distributions of the two F-POFs and their synthetic monomers are depicted in Supplementary Figure 3. The results show that the resonance signals of the aromatic monomers and the carbon atoms on the F-substituted benzene rings were detected in both polymers. It is worth noting that SPPOF-8F exhibited a signal at approximately 111 ppm, corresponding to the carbon situated at the junction of the two fluorinated benzene rings in octafluorobiphenyl. In contrast, SPPOF-4F did not display such a signal in this specific region. The thermal stability of both POFs was assessed using TGA [Supplementary Figure 4], and the findings indicated that both SPPOF-4F and SPPOF-8F demonstrated exceptional thermal stability with decomposition temperatures exceeding 350 °C in an air atmosphere. We performed contact angle tests on the two adsorbents and found that SPPOF-8F,

which has a higher fluoride content, exhibited greater hydrophobicity compared to SPPOF-4F [Supplementary Figure 5].

SEM was utilized to examine the microscopic morphology of SPPOF-4F and SPPOF-8F. As depicted in Figure 2, both F-POFs exhibited irregular morphologies [Figure 2A and C]. Based on this, the composition and dispersibility of various elements within the F-POFs were examined using EDS analysis, with the results presented in Supplementary Figure 6A-D. It is clear that F is evenly distributed in both F-POFs. Additionally, the C/F atomic ratios of SPPOF-4F and SPPOF-8F are approximately 5.02 and 2.92 [Figure 2B and D], respectively, which closely align with the theoretical C/F atomic ratios for the two F-POFs (C/F = 4.62 for SPPOF-4F and C/F = 2.31 for SPPOF-8F), confirming that the synthesized F-POFs met expectations.

N_2 adsorption tests were conducted on SPPOF-4F and SPPOF-8F at 77 K, and the resulting adsorption-desorption isotherms are presented in Figure 3A and B. It can be seen that both F-POFs exhibit characteristic Type IV adsorption isotherms with hysteresis in the desorption. Based on the N_2 adsorption isotherms at 77 K and the Brunauer-Emmett-Teller (BET) adsorption type, the specific surface areas of SPPOF-4F and SPPOF-8F were calculated to be 915 $m^2 \cdot g^{-1}$ and 971 $m^2 \cdot g^{-1}$, respectively. Meanwhile, the non-local density functional theory (NLDFT) model was employed to calculate the pore size distribution (PSD) of two F-POFs, as depicted in Figure 3C and D. It is evident that the main pore sizes of SPPOF-4F and SPPOF-8F are concentrated at 1.35 and 1.55 nm, respectively, with some mesopores in 2-10 nm, proving that both SPPOF-4F and SPPOF-8F are typical micro-mesoporous materials[50].

Single-component adsorption

As shown in Figure 4, the single-component adsorption isotherms of C_2F_6 and CF_4 were tested at 273 K and 298 K for SPPOF-4F and SPPOF-8F, respectively. The adsorption capacities of SPPOF-4F and SPPOF-8F for C_2F_6 exhibited a significantly higher affinity compared to that for CF_4. At 273 K, the adsorption capacities of C_2F_6 in SPPOF-4F and SPPOF-8F were found to be 39.0 and 40.9 mL/g, respectively. In comparison, the uptake of CF_4 in SPPOF-4F and SPPOF-8F under identical conditions yielded adsorption capacities of 17.8 and 16.0 mL/g, respectively. Besides, the adsorption isotherms of C_2F_6 showed a rapid upward trend throughout the adsorption range, while the adsorption isotherms of CF_4 were almost linear. Furthermore, it was observed that the adsorption of C_2F_6 by both F-POFs at 273 K exceeded that at 298 K, with complete desorption of C_2F_6 occurring upon pressure reduction, indicating a typical physical adsorption process for C_2F_6 in SPPOF-4F and SPPOF-8F. We also conducted a comparative analysis of the C_2F_6/CF_4 separation performance of adsorbents reported in the existing literature. The findings indicate that while SPPOFs may not exhibit the highest adsorption capacity for C_2F_6, their separation selectivity for C_2F_6/CF_4 surpasses that of most documented adsorbents. This suggests that SPPOFs hold significant potential for CF_4 purification applications. Detailed results can be found in Supplementary Table 1.

Isosteric heat of adsorption

The Q_{st} is widely used to evaluate the thermodynamic adsorption affinity of an adsorbent toward a gas molecule. Herein, the Q_{st} of C_2F_6 and CF_4 were determined using the Virial equation based on adsorption isotherms. The Q_{st} curves of SPPOF-4F and SPPOF-8F for the two gases show different trends, as shown in Figure 5. Specifically, at near-zero coverage, the Q_{st} values of SPPOF-4F for C_2F_6 and CF_4 are 29.0 and 20.5 kJ/mol, respectively [Figure 5A]. Similar results are also observed for SPPOF-8F with Q_{st} values of 28.5 and 11.4 kJ/mol for C_2F_6 and CF_4, respectively, at near-zero coverage [Figure 5B]. The results indicate that the thermodynamic affinity of both F-POFs for C_2F_6 is greater than that for CF_4. In contrast, the difference in the Q_{st} values of SPPOF-8F for C_2F_6 and CF_4 is larger than that of SPPOOF-4F in total coverage, suggesting that SPPOOF-8F shows higher adsorption affinity in a different C_2F_6/CF_4 gas mixture.

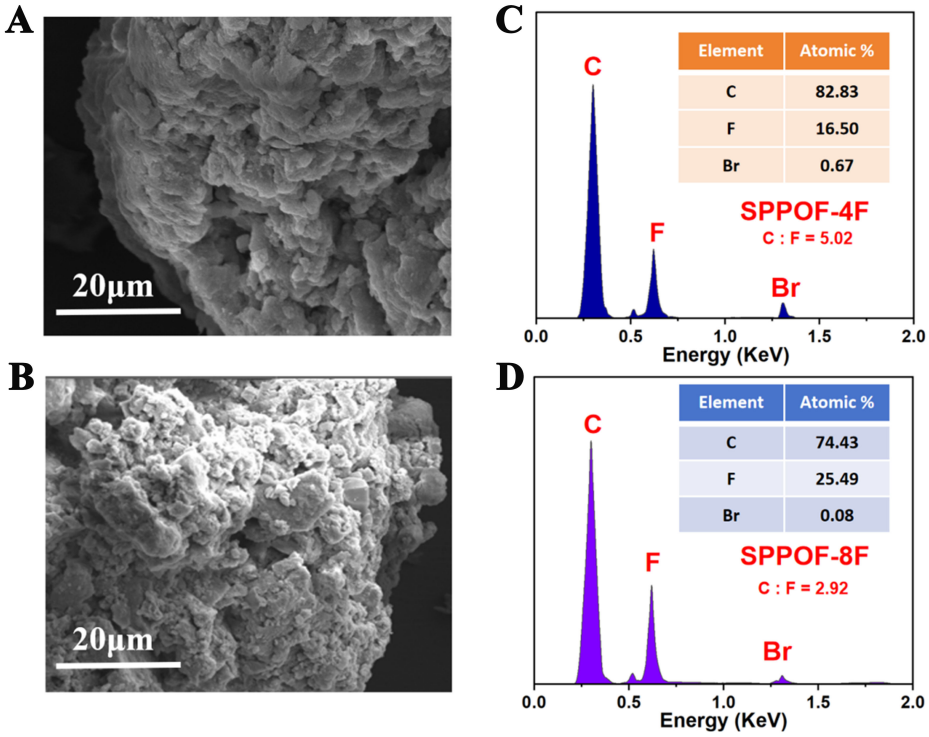

Figure 2. Morphology images of (A) SPPOF-4F and (B) SPPOF-8F obtained by SEM; EDS analysis curves for (C) SPPOF-4F and (D) SPPOF-8F. SEM: Scanning electron microscopy; EDS: energy dispersive spectroscopy.

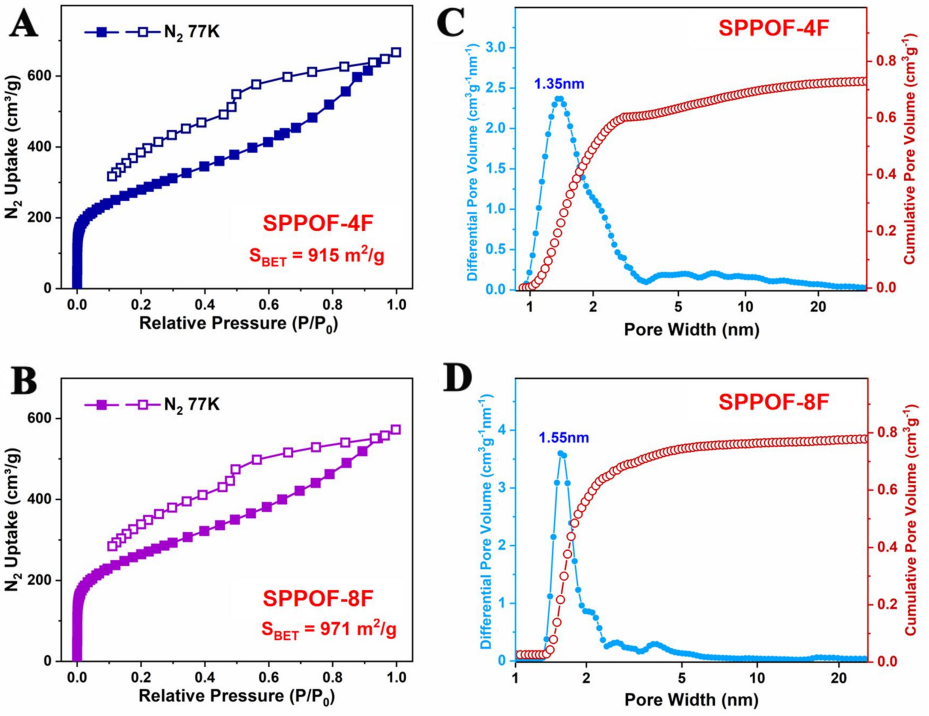

Figure 3. N_2 adsorption and desorption isotherms: (A) SPPOF-4F and (B) SPPOF-8F. PSD calculated by NLDFT method: (C) SPPOF-4F and (D) SPPOF-8F. PSD: Pore size distribution; NLDFT: non-local density functional theory.

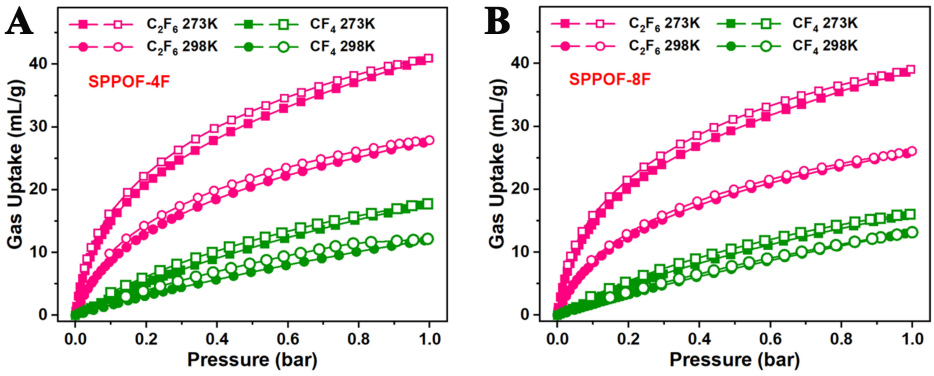

Figure 4. Adsorption and desorption isotherms of C_2F_6 and CF_4 in (A) SPPOF-4F and (B) SPPOF-8F at 273 and 298 K.

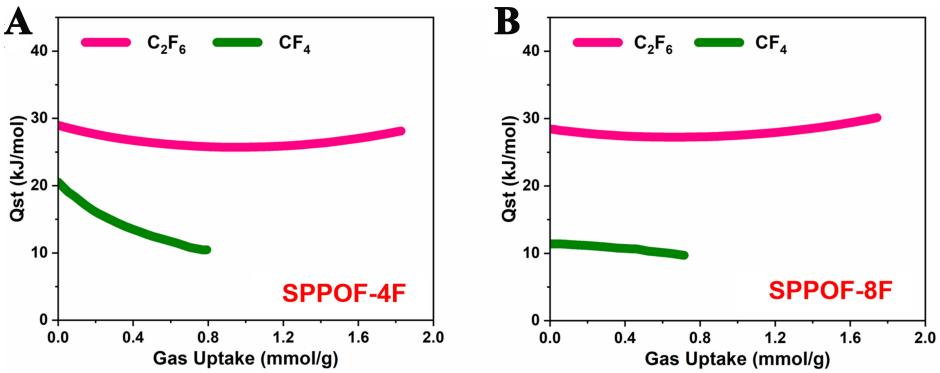

Figure 5. Q_{st} of (A) SPPOF-4F and (B) SPPOF-8F for C_2F_6 and CF_4.

Adsorption selectivity

To predict the separation efficiency of SPPOF-4F and SPPOF-8F for gas mixtures (C_2F_6 and CF_4), C_2F_6/CF_4 ideal adsorption solution theory (IAST) selectivity was determined by fitting the adsorption isotherms with the Langmuir-Freundlich model. Figure 6A and B shows the IAST selectivity of F-POFs for C_2F_6/CF_4 at different ratios (C_2F_6 gas content from 1% to 99%). At 298.15 K and 1 bar, SPPOF-4F and SPPOF-8F demonstrate maximum IAST selectivity for C_2F_6/CF_4 at low C_2F_6 gas concentration (C_2F_6 : CF_4 =1:99, v/v) with values of 6.72 and 8.26, respectively. As the percentage of C_2F_6 in the mixture increases to 99%, the IAST selectivity of C_2F_6/CF_4 decreases to 4.90 and 5.98 for SPPOF-4F and SPPOF-8F, respectively. The IAST selectivity demonstrates a consistent decrease with the increase in the percentage of C_2F_6 in the gas mixture. It is worth mentioning that higher fluorine content of SPPOF-8F leads to a stronger F-induced interaction force between the F-POFs and C_2F_6, resulting in its higher IAST selectivity compared to that of SPPOF-4F for mixed gases across all compositions.

Time-dependent adsorption kinetics

In order to investigate the kinetic adsorption of gas in F-POFs, we conducted tests on the adsorption rates of C_2F_6 and CF_4 in SPPOF-4F and SPPOF-8F at 298.15 K and 1 bar. As depicted in Figure 7, both SPPOF-4F and SPPOF-8F exhibit initial high adsorption rates for both gases, followed by a rapid decrease with increasing adsorption time. The maximum adsorption rates of SPPOF-4F for C_2F_6 and CF_4 were 20.4 and 8.0 $mL \cdot g^{-1} \cdot s^{-1}$, respectively [Figure 7A and B], while the maximum adsorption rates of SPPOF-8F for C_2F_6 and CF_4 were 20.0 and 11.0 $mL \cdot g^{-1} \cdot s^{-1}$, respectively [Figure 7C and D]. Interestingly, both SPPOF-4F and SPPOF-8F showed higher adsorption rates of C_2F_6 than CF_4, indicating preferential adsorption of C_2F_6 into F-POFs.

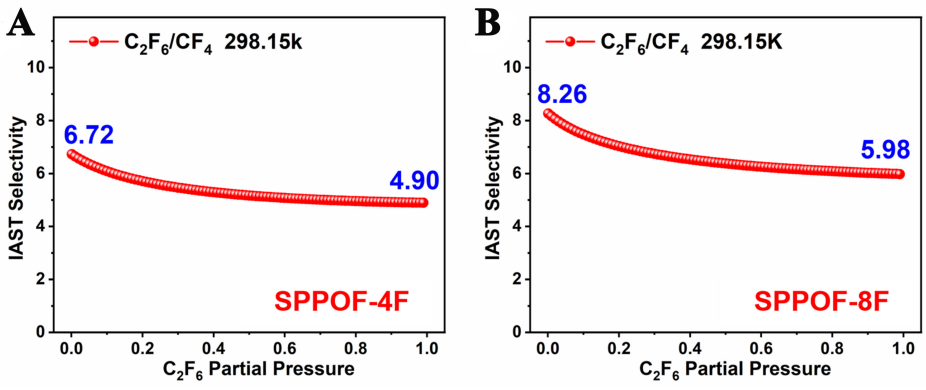

Figure 6. The IAST selectivity of (A) SPPOF-4F and (B) SPPOF-8F to various ratios of C_2F_6/CF_4 gas mixture (ranging from 1% to 99% C_2F_6) at a pressure of 1 bar and temperature of 298.15 K. IAST: Ideal adsorbed solution theory.

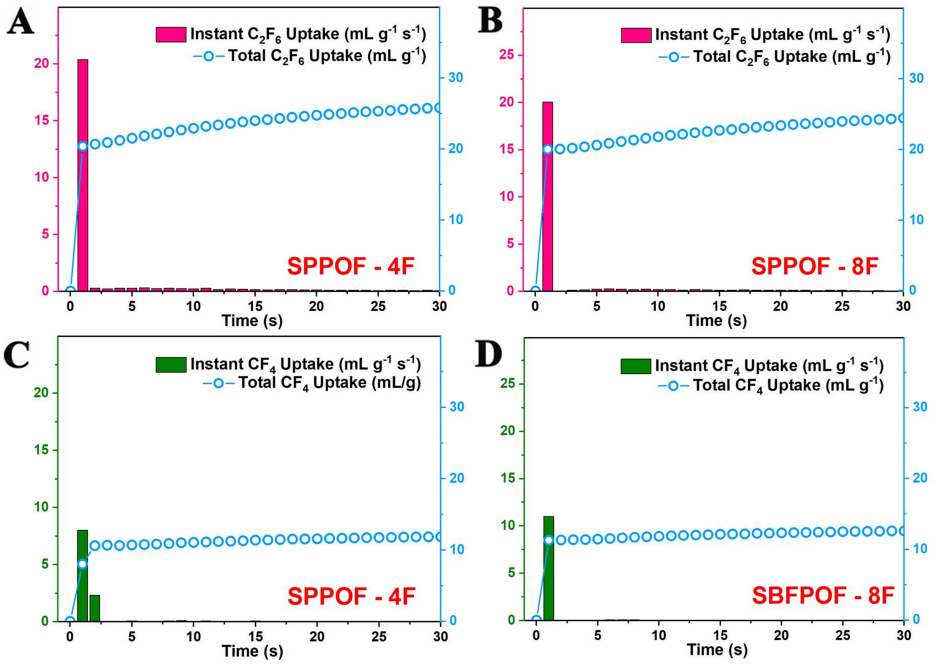

Figure 7. Time-dependent adsorption kinetics of (A) C_2F_6 and (B) CF_4 in SPPOF-4F and adsorption rates of (C) C_2F_6 and (D) CF_4 in SPPOF-8F at 298.15 K under 1 bar.

Dynamic breakthrough experiments

In order to assess the practical applicability of SPPOF-4F and SPPOF-8F, breakthrough experiments were conducted at 298.15 K to investigate the dynamic separation of C_2F_6/CF_4 gas mixtures. The feed gas consisted of a 1:1 (v/v) volume ratio mixture of C_2F_6 and CF_4, with a constant flow rate of 80 mL/min. Gas composition was monitored using an INFICON Mass spectrometer. In Figure 8, it is shown that during the test, CF_4 initially passed through the packed column until the relative concentrations of both CF_4 and C_2F_6 stabilized at around 1. For SPPOF-4F, CF_4 reached adsorption saturation at 2.4 min/g after the start of the experiment, while the adsorption saturation time for C_2F_6 was 5.1 min/g [Figure 8A]. In contrast, for SPPOF-8F, CF_4 reached adsorption saturation at 2.9 min/g after the beginning of the experiment, whereas

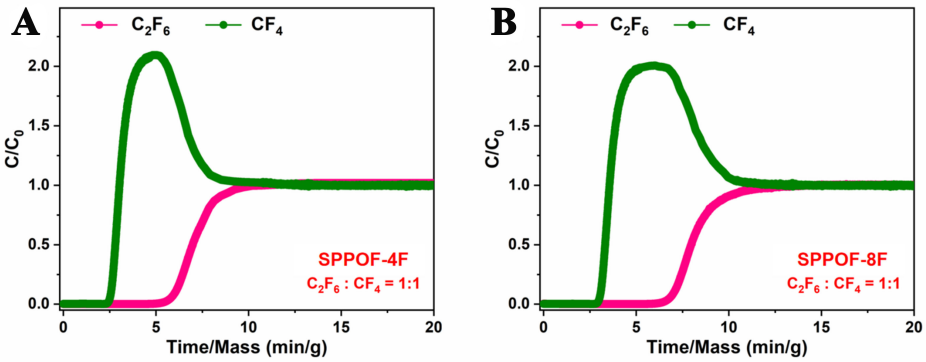

Figure 8. Breakthrough curves of C_2F_6/CF_4 gases mixture in (A) SPPOF-4F and (B) SPPOF-8F.

C_2F_6 adsorption saturated at up to 6.3 min/g [Figure 8B]. The adsorption saturation time for C_2F_6 was significantly longer than that for CF_4 for both polymers, which further confirms the potential of samples in separating C_2F_6. It is noteworthy that the time windows for the purification of CF_4 by the two F-POFs were relatively limited, approximately 2.7 min/g for SPPOF-4F and 3.4 min/g for SPPOF-8F, which may be attributed to the utilization of a shorter packing column in this experimental setup.

Theoretical simulation and calculation of gas adsorption mechanism

Theoretical calculations employing DFT were conducted to enhance our comprehension of the adsorption mechanism of C_2F_6 and CF_4 in F-POFs. Repetitive structural unit fragment models of the polymers were constructed using Material Studio Visualizer, and calculations were performed with the DMol³ module. The electrostatic potential distribution of the gas molecules and POFs structural units was computed using Mulliken analysis, as depicted in Figure 9A-D. The blue region represents areas of low potentials, while the red-covered region indicates high potentials. The intensity of the color is indicative of the magnitude of the electrostatic potentials. Notably, a dark blue color is observed in the region where the F atoms are located, signifying a strong negative potential. Simultaneously, the center of the benzene ring and the H atoms are depicted in red, indicating high positive potential. The introduction of F atoms apparently induces polarization in the porous polymer, resulting in a potential gradient on the pore surface. This enhances the electrostatic force exerted by the polymer on the C_2F_6 molecule due to the presence of positive potential centers[51,52]. Additionally, C_2F_6 molecules with more F atoms have a stronger negative electric field than CF_4, so theoretically F-POFs have a stronger affinity for C_2F_6.

Based on the above results, we constructed adsorption models for the two F-POFs with C_2F_6 and CF_4, as illustrated in Figure 9E-H. The electrostatic potential simulation shows that gas molecules preferentially adsorb near the benzene ring with a positive potential [Supplementary Figure 7]. The simulation results of Mulliken atomic charge indicate that the charge transfer induced by SPPOF-8F with a higher F content to C_2F_6 is 0.0046 (a.u.), which is significantly greater than the 0.0016 (a.u.) observed for SPPOF-4F [Supplementary Table 2]. These findings suggest that a higher F content contributes to the enhancement of electrostatic interaction between F-POFs and C_2F_6. DFT calculations show that the absolute values of the E_{Int} for both SPPOF-4F and SPPOF-8F with C_2F_6 are larger than those with CF_4 (-43.42 *vs.* -23.09 kJ/mol and -46.12 *vs.* -26.01 kJ/mol). Overall, it can be inferred that the high selective adsorption separation of C_2F_6/CF_4 in two F-POFs is attributed to the unique affinity of their positive potential points for the more electronegative C_2F_6 gas through electrostatic interaction.

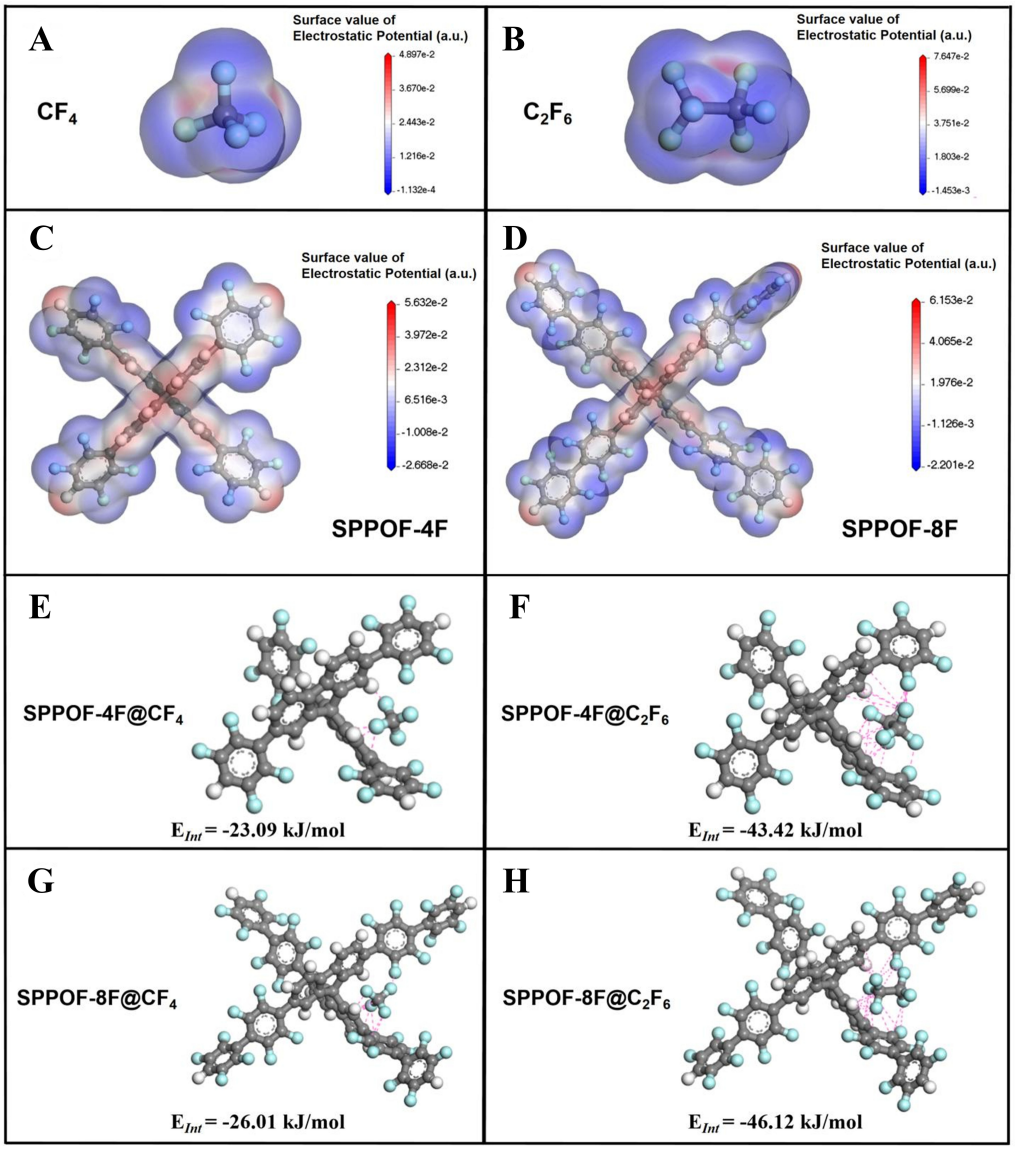

Figure 9. Simulated structures and the electrostatic potential maps of (A) CF_4, (B) C_2F_6, (C) SPPOF-4F and (D) SPPOF-8F; The E_{Int} between the POFs and gas molecules: (E) SPPOF-4F@CF_4, (F) SPPOF-4F@C_2F_6, (G) SPPOF-8F@CF_4 and (H) SPPOF-8F@C_2F_6. POFs: Porous organic frameworks.

Evaluation of reusability and stability

The practical application requires crucial considerations of the reusability and stability of adsorbents; as illustrated in Figure 10A, it is evident that the adsorption capacity of SPPOF-8F for C_2F_6 and CF_4 remained relatively constant after six consecutive cycling tests at 298 K, demonstrating excellent reusability and stability of both F-POFs. In addition, we soaked the two POFs in 1 M hydrochloric acid and 1 M NaOH solutions at room temperature for two days to evaluate their chemical stability. The treated samples were subsequently gathered, analyzed using FT-IR, and exposed to C_2F_6 adsorption trials at 298 K and 1 bar. Additionally, the C_2F_6 adsorption isotherms [Figure 10B and C] and FT-IR spectra [Supplementary Figure 8] of the two POFs treated with HCl and NaOH exhibited minimal changes compared to those before treatment, indicating strong resistance to acid and alkali for the F-POFs.

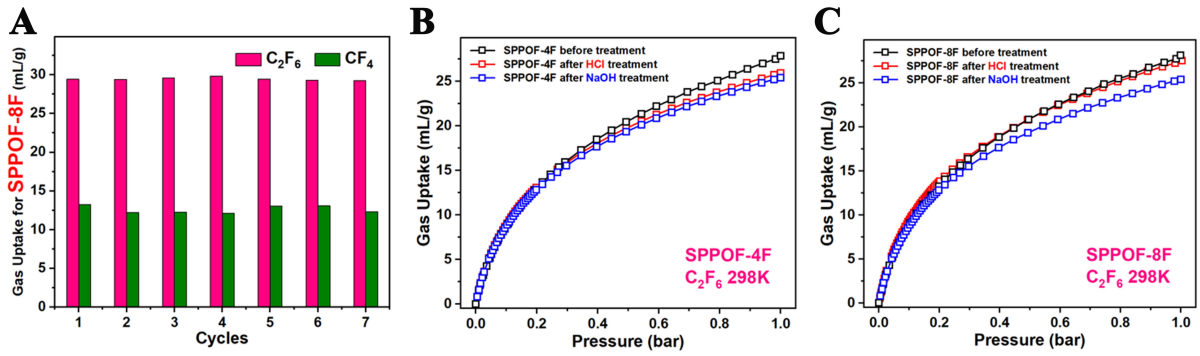

Figure 10. (A) Cyclic adsorption tests of C_2F_6 and CF_4 in SPPOF-8F at 298.15 K and 1 bar; Comparison of C_2F_6 adsorption isotherms of POFs before and after HCl or NaOH treatment: (B) SPPOF-4F and (C) SPPOF-8F at 298 K. POFs: Porous organic frameworks.

CONCLUSIONS

In this study, two F-POFs were synthesized and exhibited high adsorption selectivity for C_2F_6/CF_4 separation. The adsorption capacities of SPPOF-8F for C_2F_6 and CF_4 were 40.9 and 16.0 mL/g at 273 K and 1 bar, with the IAST selectivities as high as 8.26 (C_2F_6 : CF_4 =1:99, v:v). The C_2F_6 adsorption affinity of two POFs was verified through heat of adsorption calculation and time-dependent adsorption rate experiments. Breakthrough experiments also demonstrated the ability of F-POFs to purify CF_4. DFT calculations elucidated the adsorption mechanism of F-POFs for C_2F_6 gas at the molecular level, demonstrating that the adsorption selectivity of POFs for C_2F_6/CF_4 is achieved through F-induced electrostatic interaction at the F-POF surface. Our study serves as a reference indicating the potential applications of F-POFs in purifying CF_4 from a C_2F_6/CF_4 mixture.

DECLARATIONS

Authors' contributions

Designed the research, wrote the paper: Ma H, Li Y
Carried out the experiments and tests: Li Y
Assisted in data analysis and theoretical calculations: Wu Y, Zhang W
Programming calculations for Q_{st} and IAST selectivity: Fu Y
Participated in the characterization of materials: Wu Y, Wang S, Li X, Zeng J
Supervised the project: Ma H

Availability of data and materials

The authors confirm that the data supporting the findings of this study are available within the article and its Supplementary Materials (testing and characterization of SPPOFs and supporting figures). If there is any uncertainty, we kindly advise reaching out to the corresponding author for additional clarification.

Financial support and sponsorship

The authors gratefully acknowledge the financial support of the Natural Science Foundation of China (Grant No. 22178280), the Shaanxi Province Qin Chuangyuan "Scientist + Engineer" Team Construction Project (Grant No. 2023KXJ-058), and the Fundamental Research Funds for the Central Universities (Grant No. xzy012023171). Ma H also thanks the Fundamental Research Funds for "Young Talent Support Plan" of Xi'an Jiaotong University (HG6J001) and "1000-Plan program" of Shaanxi province. We also extend our gratitude to the Instrument Analysis Center of Xi'an Jiao Tong University for the assistance test. Additionally, we gratefully acknowledge Prof. Huanyu Zhao at Jilin University for help in getting access to mass spectrometry (MS).

Conflicts of interest

All authors declared that there are no conflicts of interest.

Ethical approval and consent to participate Consent for publication

Not applicable.

Consent for publication

Not applicable.

REFERENCES

1. Chang MB, Chang JS. Abatement of PFCs from semiconductor manufacturing processes by nonthermal plasma technologies: a critical review. *Ind Eng Chem Res* 2006;45:4101-9. DOI
2. Donnelly VM. Review article: reactions of fluorine atoms with silicon, revisited, again. *J Vac Sci Technol A Vac Surf Films* 2017;35:05C202. DOI
3. Vorotyntsev AV, Petukhov AN, Trubyanov MM, et al. Progress and perspectives in high-purity substance production for semiconductor industry. *Rev Chem Eng* 2021;37:125-61. DOI
4. Illuzzi F, Thewissen H. Perfluorocompounds emission reduction by the semiconductor industry. *J Integr Environ Sci* 2010;7:201-10. DOI
5. World Semiconductor Trade Statistics. WSTS semiconductor market forecast fall 2023. Available from: https://www.wsts.org/76/103/WSTS-Semiconductor-Market-Forecast-Fall-2023. [Last accessed on 24 Jul 2024].
6. Tang Z. The synthesis technology of high purity tetrafluoromethane by fluorine and carbon. *Cryo Spec Gases* 2013;31:32-4. (in Chinese). DOI
7. Pashkevich DS, Mukhortov DA, Petrov VB, Alekseev YI, Asovich VS, Barabanov VG. Synthesis of tetrafluoromethane by graphite fluorination with elemental fluorine. *Russian J Appl Chem* 2004;77:92-7. DOI
8. Pashkevich DS, Shelopin GG, Mukhortov DA, Petrov VB, Alekseev YI, Asovich VS. Synthesis of perfluoroalkanes by high-temperature reaction of graphite with fluorine in a fluidized bed. *Russ J Appl Chem* 2004;77:1847-53. DOI
9. Chen G, Ni Z. CN101298318A Method and apparatus for preparing high-purity carbon tetrafluoride gas. 2008. Available from: https://worldwide.espacenet.com/patent/search/family/040078304/publication/CN101298318A?q=CN101298318A. [Last accessed on 24 Jul 2024].
10. Bao H, Timothy A. US5779863A Perfluoro compound (PFC) separation and purification method and system. 1997. Available from: https://worldwide.espacenet.com/patent/search/family/025129273/publication/US5779863A?q=US5779863A. [Last accessed on 24 Jul 2024].
11. Asensio-Delgado S, Pardo F, Zarca G, Urtiaga A. Absorption separation of fluorinated refrigerant gases with ionic liquids: equilibrium, mass transport, and process design. *Sep Purif Technol* 2021;276:119363. DOI
12. Vorotyntsev VM, Drozdov PN, Vorotyntsev IV, Anikin AE, Beljaev EM, Soboleva YA. The physico-chemical bases of separation and high purification of fluorocarbons and simple gases. *Pet Chem* 2011;51:492-5. DOI
13. Battisti R, Machado RA, Marangoni C. A background review on falling film distillation in wetted-wall columns: from fundamentals towards intensified technologies. *Chem Eng Process Process Intensif* 2020;150:107873. DOI
14. Ma H, Sun J, Li Z, Liu X. Research progress and optimization prospect of constant boiling distillation technology. *E3S Web Conf* 2021;290:03025. DOI
15. Wang H, Shi Z, Yang J, et al. Docking of Cu^{I} and Ag^{I} in metal-organic frameworks for adsorption and separation of xenon. *Angew Chem Int Ed Engl* 2021;60:3417-21. DOI PubMed
16. Wu D, Zhang P, Yang G, et al. Supramolecular control of MOF pore properties for the tailored guest adsorption/separation applications. *Coord Chem Rev* 2021;434:213709. DOI
17. Mukherjee S, Sensharma D, Qazvini OT, et al. Advances in adsorptive separation of benzene and cyclohexane by metal-organic framework adsorbents. *Coord Chem Rev* 2021;437:213852. DOI
18. Mohammed N, Lian H, Islam MS, et al. Selective adsorption and separation of organic dyes using functionalized cellulose nanocrystals. *Chem Eng J* 2021;417:129237. DOI
19. Ding Y, Alimi LO, Moosa B, et al. Selective adsorptive separation of cyclohexane over benzene using thienothiophene cages. *Chem Sci* 2021;12:5315-8. DOI PubMed PMC
20. Lv D, Zhou P, Xu J, et al. Recent advances in adsorptive separation of ethane and ethylene by C_2H_6-selective MOFs and other adsorbents. *Chem Eng J* 2022;431:133208. DOI
21. Gong W, Xie Y, Pham TD, et al. Creating optimal pockets in a clathrochelate-based metal-organic framework for gas adsorption and

separation: experimental and computational studies. *J Am Chem Soc* 2022;144:3737-45. DOI PubMed

22. Brandt P, Nuhnen A, Öztürk S, Kurt G, Liang J, Janiak C. Comparative evaluation of different MOF and non-MOF porous materials for SO_2 adsorption and separation showing the importance of small pore diameters for low-pressure uptake. *Adv Sustain Syst* 2021;5:2000285. DOI
23. Rehman A, Nazir G, Yop Rhee K, Park S. A rational design of cellulose-based heteroatom-doped porous carbons: promising contenders for CO_2 adsorption and separation. *Chem Eng J* 2021;420:130421. DOI
24. Xie W, Yang L, Zhang J, Zhao X. The adsorptive separation of ethylene from C_2 hydrocarbons by metal-organic frameworks. *Chemistry* 2023;29:e202300158. DOI PubMed
25. Guo Y, Su C, Chen H, et al. Hierarchical porous carbon with tunable apertures and nitrogen/oxygen heteroatoms for efficient adsorption and separation of VOCs. *Chem Eng J* 2023;471:144558. DOI
26. Ryu U, Jee S, Rao PC, et al. Recent advances in process engineering and upcoming applications of metal-organic frameworks. *Coord Chem Rev* 2021;426:213544. DOI PubMed PMC
27. Lee JM, Cooper AI. Advances in conjugated microporous polymers. *Chem Rev* 2020;120:2171-214. DOI PubMed PMC
28. Ma Y, Cui F, Rong H, et al. Continuous porous aromatic framework membranes with modifiable sites for optimized gas separation. *Angew Chem Int Ed Engl* 2022;61:e202113682. DOI PubMed
29. Yuan Y, Zhu G. Porous aromatic frameworks as a platform for multifunctional applications. *ACS Cent Sci* 2019;5:409-18. DOI PubMed PMC
30. Das S, Heasman P, Ben T, Qiu S. Porous organic materials: strategic design and structure-function correlation. *Chem Rev* 2017;117:1515-63. DOI PubMed
31. Bai R, Song X, Yan W, Yu J. Low-energy adsorptive separation by zeolites. *Natl Sci Rev* 2022;9:nwac064. DOI PubMed PMC
32. Peng X, Vicent-Luna JM, Jin Q. Separation of CF_4/N_2, C_2F_6/N_2, and SF_6/N_2 mixtures in amorphous activated carbons using molecular simulations. *ACS Appl Mater Interfaces* 2020;12:20044-55. DOI PubMed
33. Sosa JE, Malheiro C, Ribeiro RP, et al. Adsorption of fluorinated greenhouse gases on activated carbons: evaluation of their potential for gas separation. *J Chem Tech Biotech* 2020;95:1892-905. DOI
34. Choi SW, Yoon HJ, Lee HJ, Lee E, Lim D, Lee KB. CF_4 adsorption on porous carbon derived from silicon carbide. *Microporous Mesoporous Mater* 2020;306:110373. DOI
35. Zhu J, Hu J, Xiao H, et al. Aluminum-based metal organic frameworks for greenhouse gases CF_4 and C_2F_6 capture with excellent capacity and selectivity. *Sep Purif Technol* 2024;331:125614. DOI
36. Chuah CY, Goh K, Bae TH. Hierarchically structured HKUST-1 nanocrystals for enhanced SF_6 capture and recovery. *J Phys Chem C* 2017;121:6748-55. DOI
37. Kim MB, Lee SJ, Lee CY, Bae YS. High SF_6 selectivities and capacities in isostructural metal-organic frameworks with proper pore sizes and highly dense unsaturated metal sites. *Microporous Mesoporous Mater* 2014;190:356-61. DOI
38. Senkovska I, Barea E, Navarro JAR, Kaskel S. Adsorptive capturing and storing greenhouse gases such as sulfur hexafluoride and carbon tetrafluoride using metal-organic frameworks. *Microporous Mesoporous Mater* 2012;156:115-20. DOI
39. Kim M, Kim K, Kim T, et al. Highly selective adsorption of SF_6 over N_2 in a bromine-functionalized zirconium-based metal-organic framework. *Chem Eng J* 2018;339:223-9. DOI
40. Guo Y, Tan C, Sun J, Li W, Zhang J, Zhao C. Porous activated carbons derived from waste sugarcane bagasse for CO_2 adsorption. *Chem Eng J* 2020;381:122736. DOI
41. Jiang N, Shang R, Heijman SGJ, Rietveld LC. High-silica zeolites for adsorption of organic micro-pollutants in water treatment: a review. *Water Res* 2018;144:145-61. DOI PubMed
42. Xu X, Megarajan SK, Zhang Y, Jiang H. Ordered mesoporous alumina and their composites based on evaporation induced self-assembly for adsorption and catalysis. *Chem Mater* 2020;32:3-26. DOI
43. Wu J, Xu F, Li S, et al. Porous polymers as multifunctional material platforms toward task-specific applications. *Adv Mater* 2019;31:e1802922. DOI PubMed
44. Chaoui N, Trunk M, Dawson R, Schmidt J, Thomas A. Trends and challenges for microporous polymers. *Chem Soc Rev* 2017;46:3302-21. DOI PubMed
45. Farha OK, Yazaydın AÖ, Eryazici I, et al. De novo synthesis of a metal-organic framework material featuring ultrahigh surface area and gas storage capacities. *Nat Chem* 2010;2:944-8. DOI PubMed
46. Comotti A, Castiglioni F, Bracco S, et al. Fluorinated porous organic frameworks for improved CO_2 and CH_4 capture. *Chem Commun* 2019;55:8999-9002. DOI
47. Wu AX, Drayton JA, Mizrahi Rodriguez K, et al. Elucidating the role of fluorine content on gas sorption properties of fluorinated polyimides. *Macromolecules* 2021;54:22-34. DOI
48. Feng L, Guo J, Zhong X, Sun Z. Fluorinated porous poly(spirobifluorene) via direct C-H arylation: characterization, porosity, and gas uptake. *J Macromol Sci Part A* 2014;51:604-9. DOI
49. Boopalachandran P, Laane J. Vibrational spectra, structure, and theoretical calculations of 2-fluoro- and 3-fluoropyridine. *Spectrochim Acta A Mol Biomol Spectrosc* 2011;79:1191-5. DOI PubMed
50. Al-Ghouti MA, Da'ana DA. Guidelines for the use and interpretation of adsorption isotherm models: a review. *J Hazard Mater* 2020;393:122383. DOI PubMed
51. Bai X, Wang X, Lu X, et al. A fluorine induced enhancement of the surface polarization and crystallization of g-C_3N_4 for an efficient charge separation. *New J Chem* 2021;45:9334-45. DOI
52. Werner P, Wächter T, Asyuda A, et al. Electron transfer dynamics and structural effects in benzonitrile monolayers with tuned dipole moments by differently positioned fluorine atoms. *ACS Appl Mater Interfaces* 2020;12:39859-69. DOI